Comparison of laser irradiation behavior of plasma-sprayed Ba2-xSrxSmTaO6 coatings

Jiayi Zheng (676784586@qq.com)
Beijing Institute of Technology https://orcid.org/0000-0002-3425-0353
Zhuang Ma
Beijing Institute of Technology College of Chemistry and Chemical Engineering
Yanbo Liu
Beijing Institute of Technology
Lihong Gao
Beijing institute of technology

Research Article

Keywords: Laser irradiation; plasma spray; protection threshold; perovskite; thermal barrier

Posted Date: April 29th, 2020

DOI: https://doi.org/10.21203/rs.3.rs-25065/v1

Abstract

$Ba_{2-x}Sr_xSmTaO_6$ (x = 0–2), a series of low thermal conduction and good thermal stability materials, is believed to have potential use as thermal insulation laser protection materials, however, is limited by their unclear laser damage mechanism. Thus, in this paper, we investigated and compared their laser damage behaviors as well as their protection thresholds. The $Ba_{2-x}Sr_xSmTaO_6$ (x = 0, 0.5, 1, 1.5 and 2) powder were prepared by solid state reaction and the coatings were prepared by air plasma spray. During the laser irradiation process, we observed that the coatings underwent irradiation center turning bright, grains recrystallization and melting process. When the laser power density was 500W/cm^2, no damage was observed in all five components coatings and the ablation surface of x = 1 and 2 coatings turned bright. However, the melting phenomenon occurred to x = 0.5, 1, 1.5 and 2 coatings while the laser power density reached 1000W/cm^2, and the ablation area of x = 0 coatings started to turn bright. At 1500W/cm^2 laser power density, coatings of all five components melted and the melting area of x = 0 and 1 was obviously smaller than the coatings of other three components. Ba_2SmTaO_6 (x = 0) showed the highest protection threshold that was 2000W/cm^2 for 10 s, and x = 0.5 coatings showed the lowest protection threshold that was 1000W/cm^2 for 26 s. In terms of back surface temperature, $BaSrSmTaO_6$ (x = 1) presented the lowest value and Ba_2SmTaO_6 was only slightly higher than it. To sum up, Ba_2SmTaO_6 has the best comprehensive laser protection properties and is believed to be the most potential laser protection materials among the five components.

1. Introduction:

The term "laser" originated as an acronym for "light amplification by stimulated emission of radiation"[1, 2]. It has the characteristics of extremely small divergence, high brightness (power), good monochromaticity and coherence that has been widely used in industry, medical care, military and so on[3–5]. With the rapid development of laser technology, laser has obtained great progress and their output power can up to hundreds of kW, resulting serious threaten to production equipment and personnel during the use of laser. Therefore, the protection of production equipment and personnel is of great necessary.

Up to now, laser protection materials of various types have been reported[6–11], which can be divided into three types according to protection principle: ablated type, reflective type and thermal barrie type. Ablated type laser protection materials are always accompanied by fire and smoke during laser ablation, which may affect the cleanliness and operation of equipment. While reflective protection materials often exist in the form of thin films usually with complex preparation process, and their low protection threshold determines they only suitable for the protection of weak lasers such as goggles and some optical device[12]. Thermal barrier type laser protection materials are relied on the low thermal conductivities of thermal barrier materials, which can reduce the temperature of protected substrates during laser loading. No serious chemical reaction will appear in laser ablation process and is helpful to the stable operation of equipment. In addition, most of the thermal barrier materials are ceramic

materials[13, 14], which have good thermal stability and can be used at extremely high temperatures. Thus, compared to other two types, materials of thermal barrier type have great advantages to be used in high power laser protection.

Rare earth tantalate possess comparable thermal condition and much more excellent high temperature stability compared to YSZ (Y_2O_3-stabilized ZrO_2), which have attracted lots of attention in thermal barrier area [15–17]. Among them, $Ba_{2-x}Sr_xSmTaO_6$ has low thermal conduction that is only 1-1.35W/m·K from room temperature to 1200℃ (YSZ 2.5W/m·K, 1000℃) and its thermal expansion coefficient is $8.6–9.4 \times 10^{-6} K^{-1}$, which is close to metal substrate (YSZ ~ $10 \times 10^{-6} K^{-1}$). Therefore, it is believed to be a promising candidate for thermal barrier coatings and also has the potential to become laser protection material. However, up to now, researches about $Ba_{2-x}Sr_xSmTaO_6$ have only involved its crystal structures, thermal and dielectric properties[18, 19], and its mechanism of laser damage and protection thresholds have not been studied.

In this paper, $Ba_{2-x}Sr_xSmTaO_6$ (x = 0, 0.5, 1, 1.5, 2) coatings were prepared by plasma spray. Plasma spray owns many advantages in coating deposition such as wide range of spraying materials, strong bonding strength and good adaptability of coatings, making it widely used in the preparation of coatings served in extreme service conditions. The prepared coatings were irradiated by high-intensity continuous laser with 1064 nm wavelength and the phase structures, microstructures, ablation behavior and protection thresholds were investigated respectively.

2. Experimental Method

$Ba_{2-x}Sr_xSmTaO_6$ (x = 0, 0.5, 1, 1.5 and 2) powder were prepared in muffle furnace by conventional solid reaction method with initial materials $BaCO_3$(99% purity, Sinopharm Chemical ReagentCo, China),$SrCO_3$(99% purity, Sinopharm Chemical ReagentCo, China), Sm_2O_3(99.9% purity, Rare-chem hi-tech Co., Huizhou, China) and Ta_2O_5(Ningxia Orient Ta Ind Co,Ningxia, China). Before weighted, Sm_2O_3 was preheated at 900℃ for 2 hours to remove the absorbed moisture and other gases, and $BaCO_3$, $SrCO_3$, Ta_2O_5 was dried at 120℃ for at least 24 hours. Powders were weighed by stoichiometric quantities and mixed in ethanol medium, and subsequently ball-milled in a planetary mill for 6–8 h. After drying, the mixed powder was sintered at 1200℃ for 8 hours with a heating rate of 5℃/min and furnace cooling.

Disk-shaped stainless steel (Ø25.4 mm × 10 mm) was used as substrate. The top surface of the substrate was cleaned by acetone and grit blasted with 40-mesh alumina grit under the pressure of 0.2 MPa to strengthen the adhesion between the bond layer and substrate. The NiCrCoAlY powder (Co-210, Praxair), as an approximately 100 μm thick bond layer, was deposited by high-velocity oxygen fuel spray on the blasted top surface of the substrate using Praxair JP5000. Then, the deposition of $Ba_{2-x}Sr_xSmTaO_6$ coating was performed using a plasma spray system (GTS-5500, Praxair, America) equipped with an SG-100 torch, with Ar and He as the primary and secondary gases, respectively. The primary, secondary and carrier gas were set as 90 scfh, 25 scfh and 8 scfh, respectively. The current was set as 800 A and the

powder feed rate was 20 g/min. Besides, the distance between spray gun and samples was 100 mm, and the moving speed was 500 mm/s.

The phase structures of coatings were confirmed by X-ray diffraction (XRD) using X'Pert PRO MPD. The microstructures of coatings were analyzed based on an S-4800 scanning electron microscope (SEM). An ytterbium continuous laser system with 1070 nm wavelength in a 10 × 10 mm laser spot was used for laser irradiation. The front-surface scattered light of coatings was collected by computer system equipped with an InGaAs detector. The evolution of ablation behaviors was studied under different laser parameters (power density: 500, 1000 and 1500 W/cm^2, irradiation time: 5 and 10 s). In order to further investigate their laser irradiation thresholds, tougher conditions that means higher laser power density (2000 W/cm^2) or longer duration time (30 s) were also adopted.

3. Results And Discussion

3.1 Plasma sprayed $Ba_{2-x}Sr_xSmTaO_6$ coatings

The XRD patterns before and after plasma spray are shown in Fig. 1. Figure 1a and 1c show the phase structures of $Ba_{2-x}Sr_xSmTaO_6$ powders before plasma spray. Before plasma spray, powders of all the five components have single phase structure (Fig. 1a), and no second phase was observed. With the increase of Sr doping contents, the peaks of $Ba_{2-x}Sr_xSmTaO_6$ move toward high angle direction (Fig. 1a in blue and Fig. 1c), indicating the crystal lattices decrease with Sr doping content. It is because Sr ions are smaller than Ba ions that leads to the decrease of crystal lattices. This phenomenon is also confirmed by the results of first principle calculations[20]. Some weak peaks at around 18° (in red circles) are visible, which are related to the order structures of B site. Another notable phenomenon is that the peaks of x = 0 and 2 powders at around 30° split to several peaks (clearly in Fig. 1c), which is different from the symmetrical single peaks of other three components. Similar phenomenon was also observed at 54° and 63°. That indicates the symmetry of Ba_2SmTaO_6 and Sr_2SmTaO_6 (x = 0 and 2) powders is lower than the other three components. After comparison with standard patterns, Ba_2SmTaO_6 and Sr_2SmTaO_6 powder is believed to have tetragonal and monoclinic phase structures respectively, instead of standard cubic perovskite structure. While when x value is 0.5, 1 and 1.5, $Ba_{2-x}Sr_xSmTaO_6$ is standard cubic perovskite structure.

The XRD patterns of $Ba_{2-x}Sr_xSmTaO_6$ coatings are shown in Fig. 1b and 1d. After plasma spray, $Ba_{2-x}Sr_xSmTaO_6$ coatings maintained the same components with the original powders, indicating no decomposition appeared during deposition. The peaks located at 18° still visible in coatings, that means both powders and coatings are B site order perovskites. For x = 0.5–1.5, their phase structures remain unchanged that means maintain standard cubic structures. While for x = 0 and 2, as shown in Fig. 1d, after plasma spray the split peaks disappeared. It indicates that during plasma spray, thanks to the high flame temperature, Ba_2SmTaO_6 and Sr_2SmTaO_6 underwent a phase transition process, and their phase

structures changed from tetragonal/monoclinic to cubic structure. Owing to the rapid cooling process after spray, their coatings maintained the high temperature cubic phase structure.

The single particle deposition, surface and cross section morphology are shown in Fig. 1e. Besides, the average thickness, porosity and reflectivity in 1064 nm of $Ba_{2-x}Sr_xSmTaO_6$ coatings were also summarized in Fig. 1e. As shown in Fig. 1e, the particles of all five components are well-melted and no unmelted particles was observed. The coatings are bonded well with substrate and their average thickness are around 200 μm. Their porosity ranges from 20–35% which is relatively high in plasma spray. It is because relatively high porosity is benefit to improve coatings' thermal barrier ability, which plays advantage role in protecting substrates. Their reflectivity at 1064 nm does not show significant difference with the change of x value, which ranges from 37–45%. The results indicate compared to reflective type protection materials, the coupling coefficient between laser and $Ba_{2-x}Sr_xSmTaO_6$ coatings are relatively high, which may cause adverse effects to laser protection.

3.2 Laser ablation behavior of $Ba_{2-x}Sr_xSmTaO_6$ coatings

When irradiated at 1000W/cm^2, the x = 0 coatings still remained unchanged after irradiated both for 5 s and 10 s. For x = 1 coatings, after irradiated for 5 s, bright phenomenon appeared in irradiation center and very tiny melting spot about 2.57mm^2 was observed. The melting phenomenon was also observed in x = 0.5, 1.5 and 2 coatings, and the melting size for 5 s is 51.82mm^2, 41.52mm^2 and 68.96mm^2 respectively, which is much larger than x = 1 coatings. When irradiated for 10 s, combined with the data listed in Table 1, we found that with the extension of irradiation time, the size of melting zone did not enlarge significantly. Because caused by the low thermal conduction, $Ba_{2-x}Sr_xSmTaO_6$, coatings have no time to conduct the laser energy to none irradiation area at the beginning of laser irradiation, resulting the rapidly increase of surface temperature. The surface temperature reaches to the melting point in a very short time, then melting occurs. With the increase of irradiation time, none irradiation zone of coatings as well as the substrate shared a lot of laser energy, therefore, the melting area dose not expand rapidly.

When the laser power density increases to 1500W/cm^2, melting phenomenon was observed in all five components coatings. After 5 s, coatings of x = 0.5, 1.5 and 2 have larger melting area than x = 0 and 1 that is 84.49mm^2, 90.85mm^2 and 100.94mm^2, respectively, followed by x = 1 (24.25mm^2) coating. The melting spot of x = 0 coating is very tiny, only 4.21mm^2. With the increasing of irradiation time, the melting zone of x = 0.5, 1.5 and 2 coatings enlarged slightly. For x = 0 and 1 coatings, the enlarge of melting zone is more obviously but still half the area of x = 0.5, 1.5 and 2 coatings. In general, from the macro morphology, coatings of x = 0 and 1 have better laser protection properties, because under the same conditions, their melting zone is smaller and melting phenomenon just occurs in higher power density conditions.

In order to investigate more detailed, sample of x = 1 component irradiated at 1500W/cm^2 for 5 s was chosen as a typical example and its micro morphology was analyzed. The results are shown in Fig. 2b and 2c. Figure 2b shows its micro morphology away from the ablation center. In this area, the coating

keeps the original spray morphology and recrystallization of grains appears in some locations (in green circle). It is caused by the effect of laser heat. In the irradiation center area (Fig. 2c), we divided it into four regions A, B, C and D. A is the most central laser irradiation area, where the coating melted during irradiation. In this region, grains are not densely connected, and large cracks and pores are observed. The grains on the most outer layer are dendritic morphology, and the grains size is about 20–40 μm. The grains behind the surface layer are equiaxed and the grains are smaller, which is about 2 μm. B is the edge of the melting zone. In this area, the grains are feather-like dendrites, with obvious directional arrangements along the direction of heat flow. The grains are dense in B region and their size become larger, about 100 μm. Besides, B region is narrow and the width is only about 100 μm. C is the edge of unmelted zone and similar to B region, C region is also very narrow with the width about 100 μm. Grains in this region are equiaxed and arranged densely with the grains size only about 2 μm. Almost no original spray morphology maintained in above three regions. D region is unmelted region but near the irradiation center. In this region, the grains recrystallized caused by the high surface temperature during irradiation. But some characteristic of original sprayed morphology still maintained. The grains here are also equiaxed and the size is even small about 1 μm.

Table 1 lists the ablation size of $Ba_{2-x}Sr_xSmTaO_6$ coatings irradiated at different laser parameter as well as their ablation thresholds. The results of ablation area have been discussed combined with macro photos above, so we only discuss the ablation thresholds in this paragraph. In order to explore the laser protection thresholds of $Ba_{2-x}Sr_xSmTaO_6$ coatings, tougher laser irradiation conditions that is 1000W/cm^2 for 30 s, 2000W/cm^2 for 5 s and 10 s, were also adopted. The protection threshold is defined as the laser irradiation parameter when the coating peels off or burns through. Except x = 0.5 coating, who was burned through at 1000W/cm^2 for 26 s, all coatings can satisfy the protection requirement of 1000W/cm^2 for 30 s. When the laser power density up to 2000W/cm^2, x = 0.5-2 coatings were burned through in the most central area at 5 s. For x = 0 coatings, the coating kept covered at 5 s, then peeled off at 10 s. Thus, in terms of protection threshold, Ba_2SmTaO_6 (x = 0) has the best laser protection ability.

Table 1
Laser ablation area and threshold of $Ba_{2-x}Sr_xSmTaO_6$

			x = 0	x = 0.5	x = 1	x = 1.5	x = 2
Ablation area / mm^2	500	5 s	0	0	0	0 (88.89)	0 (58.63)
	W/cm^2	10 s	0	0	0	0 (96.98)	0 (70.87)
	1000	5 s	0	51.82	2.57	41.52	68.96
	W/cm^2	10 s	0	53.19	3.36	50.56	84.34
	1500	5 s	4.21	84.49	24.25	90.85	100.94
	W/cm^2	10 s	53.31	102.25	55.02	97.52	115.82
Ablation threshold [W/cm^2, s]			[2000,10]	[2000,5] [1000,26]	[2000,5]	[2000,5]	[2000,5]
* Ablation area is the melting area during laser irradiation							
**The size of bright zone is in brackets							
*** Ablation threshold is the condition that the substrate expose to laser							
The XRD patterns of $Ba_{2-x}Sr_xSmTaO_6$ coatings after laser irradiation are shown in Fig. 3a (non-melting regions) and 3b (melting regions). The main phase in both the two regions is still $Ba_{2-x}Sr_xSmTaO_6$, but some peaks belongs to the second phase Sm_3TaO_7 (yellow and blue shadow) were also observed. This phenomenon is caused by the decomposition of coatings in the high temperature condition during laser irradiation. In unmelted regions, except x = 1.5 and 2 coatings, the peak of $Ba_{2-x}Sr_xSmTaO_6$ at around 18°, which is regarded as the sign of ordered perovskite structures disappeared (red circle). That means caused by the extreme high temperature during laser irradiation, the ordered structure transit to disordered structure and owing to the repaid cooling process after irradiation, the disordered structure was kept. Similar phenomenon is also observed in melted region, and in this region all five coatings have disordered structure. Furthermore, for the melting zone, the relative intensity between the peaks is also changed, which is caused by the directional crystallization in melting zone, and the results are consistent with the previous SEM analysis.								

For more comprehensive comparison, the maximum back-surface temperature of x = 0–2 coatings irradiated at different laser irradiation parameters were summarized in Fig. 3d. At low laser power density ($500W/cm^2$), the difference of back-surface temperature between x = 0–2 coatings is limited and smaller than 40℃. In this condition, the back-surface temperature of x = 0 is the highest and x = 1 is the lowest for both 5 s and 10 s. When the power density rose up to $1000W/cm^2$, the back-surface temperatures of x = 0.5, 1.5 and 2 are evidently higher than x = 0 and 1 coatings both for 5 s and 10 s. This phenomenon is related to the melting of coatings surface, which leads to the decrease of coatings reflectivity, resulting in the increase of the coupling coefficient between the laser and the coatings. This inference can be confirmed from the front-surface scattered light showed in Fig. 3f that the front-surface scattered light of x = 0.5, 1.5 and 2 at $1000W/cm^2$ showed obviously decrease trend in laser irradiation process. When the

power density is 1500W/cm^2, similar phenomenon that the back-surface temperatures of x = 0 and 1 coatings are lower than the other three was observed and the difference between them further increased, which is up to 140°C.

From the above results, we conclude Ba_2SmTaO_6 (x = 0) has the best laser protection performance, followed by $BaSrSmTaO_6$ (x = 1), and x = 0.5, 1.5 and 2 are worse. Because Ba_2SmTaO_6 has the highest laser protection threshold that is 2000W/cm^2 for 10 s compared to 2000W/cm^2 for 5 s for other four groups. Besides, the back-surface temperature of Ba_2SmTaO_6 is relatively low among the five groups which is only slightly higher than x = 1 coatings. Thus, Ba_2SmTaO_6 is believed to be the most potential materials among the five groups using in high power laser protection.

4. Conclusion

In this paper, the laser irradiation behavior of $Ba_{2-x}Sr_xSmTaO_6$ (x = 0–2) coatings was investigated. In the process of laser irradiation, the irradiation central area first turned bright, then melting occurred, finally burned through or peeled off. In the most center of melting region, grains were loose dendrites with many cracks and voids, while grains in the edge of melting region were dense and large dendrites with about 100 μm oriented along the heat flow direction. Grains in the edge of the unmelted region was recrystallized and fine equiaxed grains with about 2 μm size. Though grains in the unmelted region near the irradiation center also recrystallized, it still kept the characterization of original spray morphology. For the five coatings, at 500 W/cm^2, no melting phenomenon was observed and the irradiation center of x = 1.5 and 2 coatings started turn bright. But melting phenomenon was observed on x = 0.5, 1, 1.5 and 2 coatings at 1000W/cm^2. While at 1500W/cm^2, melting happened to all five coatings, but the melting area of x = 0.5, 1.5 and 2 coatings was twice than x = 0 and 1 coatings. In terms of protection thresholds, Ba_2SmTaO_6 (x = 0) coatings were the highest that is 2000W/cm^2 for 10 s, while x = 0.5 coatings were the lowest (1000W/cm^2 for 26 s). For back-surface temperatures, $BaSrSmTaO_6$ (x = 1) was the lowest in all tested laser irradiation parameters, and Ba_2SmTaO_6 was only slightly higher than x = 1 coatings. Thus, in summary, Ba_2SmTaO_6 coatings has the best comprehensive laser protection properties and is considered the most potential materials among the five in laser protection area.

Declarations

Funding sources:

This research did not receive any specific grant from funding agencies in the public, commercial, or not-for-profit sectors.

References

[1]. Rédei, G.P., Laser (light amplification by stimulated emission of radiation). 2008: Wiley-VCH Verlag GmbH & Co. KGaA.

[2]. J, H., Short history of laser development. Applied Optics, 2010. 25(49): p. 99-122.

[3]. Jia, G., et al., Laser three-dimensional printing microchannel heat sink for high-power diode laser array. Optical ENGINEERING, 2016(55): p. 096105.

[4]. Kim, K.S., et al., A review on research and development of laser assisted turning. International Journal of Precision Engineering & Manufacturing, 2011. 4(12): p. 753-759.

[5]. Bartkowiak, K., et al., New Developments of Laser Processing Aluminium Alloys via Additive Manufacturing Technique. Physics Procedia, 2011. part-PA(12): p. 393-401.

[6]. Li, W., et al., Multi-synergy ablative effects of laminated SiO_2-graphite/SiO_2/Cu composite irradiated by high power laser. CERAMICS INTERNATIONAL, 2019. 45(12): p. 15272-15280.

[7]. Zheng, J.W.K.L., Laser irradiation behavior of plasma-sprayed tantalum oxide coatings. Ceramics International, 2020. 3(46): p. 3875-3881.

[8]. HANSEN, S.G. and T.E. ROBITAILLE, LASER ABLATION OF A POLYSILANE MATERIAL. JOURNAL OF APPLIED PHYSICS, 1987. 62(4): p. 1394-1399.

[9]. Chaoli Fu, Y.Y.Z.H., Investigation on the laser ablation of SiC ceramics using micro-Raman mapping technique. Journal of advanced ceramics, 2016. 5(3): p. 253-261.

[10]. Zhu, J., et al., Ablation Behavior of Plasma-Sprayed $La_{1-x}Sr_xTiO_{3+\delta}$ Coating Irradiated by High-Intensity Continuous Laser. ACS APPLIED MATERIALS & INTERFACES, 2017. 9(40): p. 35444-35452.

[11]. Chen, G., et al., Laser ablation protection of polymer matrix composites by adhesive inorganic coatings. Journal of Materials Science, 2017.

[12]. Guo, Y.L., et al., Damage and protection progress of materials irradiated by laser beam. (China). Materials Protection, 2003. 12(36): p. 8-10.

[13]. Jonnalagadda, K.P., et al., Hot Corrosion Mechanism in Multi-Layer Suspension Plasma Sprayed $Gd_2Zr_2O_7$ /YSZ Thermal Barrier Coatings in the Presence of V_2O_5 + Na_2SO_4. Journal of Thermal Spray Technology, 2017. 26(1): p. 140-149.

[14]. Cherng, J.S., J.R. Sau and C.C. Chung, Aqueous electrophoretic deposition of YSZ electrolyte layers for solid oxide fuel cells. Journal of Solid State Electrochemistry, 2008. 12(7): p. 925-933.

[15]. Wang, J., et al., Microstructure and thermal properties of a promising thermal barrier coating: $YTaO_4$. 2016: p. S0272884216308124.

[16]. Peng, W., X. Chong and J. Feng, Effect of Al^{3+} doping on mechanical and thermal properties of $DyTaO_4$ as promising thermal barrier coating application. Journal of the American Ceramic Society, 2018. 5(101): p. 1818-1823.

[17]. Chen, L., et al., Synthesis and thermophysical properties of $RETa_3O_9$ (RE= Ce, Nd, Sm, Eu, Gd, Dy, Er) as promising thermal barrier coatings. Journal of the American Ceramic Society, 2018. 3(101): p. 1266-1278.

[18]. K., K.S., et al., Dilatometry and Dielectric Properties of Ba_2RTaO_6 (R= La, Pr, Sm, Dy) Ceramics. Inorganic materials, 2004. 10(40): p. 1088-1090.

[19]. Ghosh, B., S. Halder and T.P. Sinha, Dielectric Relaxation and Collective Vibrational Modes of Double-Perovskites A_2SmTaO_6 (A= Ba, Sr and Ca). Journal of the American Ceramic Society, 2014. 8(97): p. 2564-2572.

[20] Jiayi, Z., et al., Theoretical and experimental studies of Ba_2SmTaO_6 on crystal structure, electronic structure and optical properties. JOURNAL OF MATERIALS CHEMISTRY C, 2018. 6(7): p. 1806-1814.

Figures

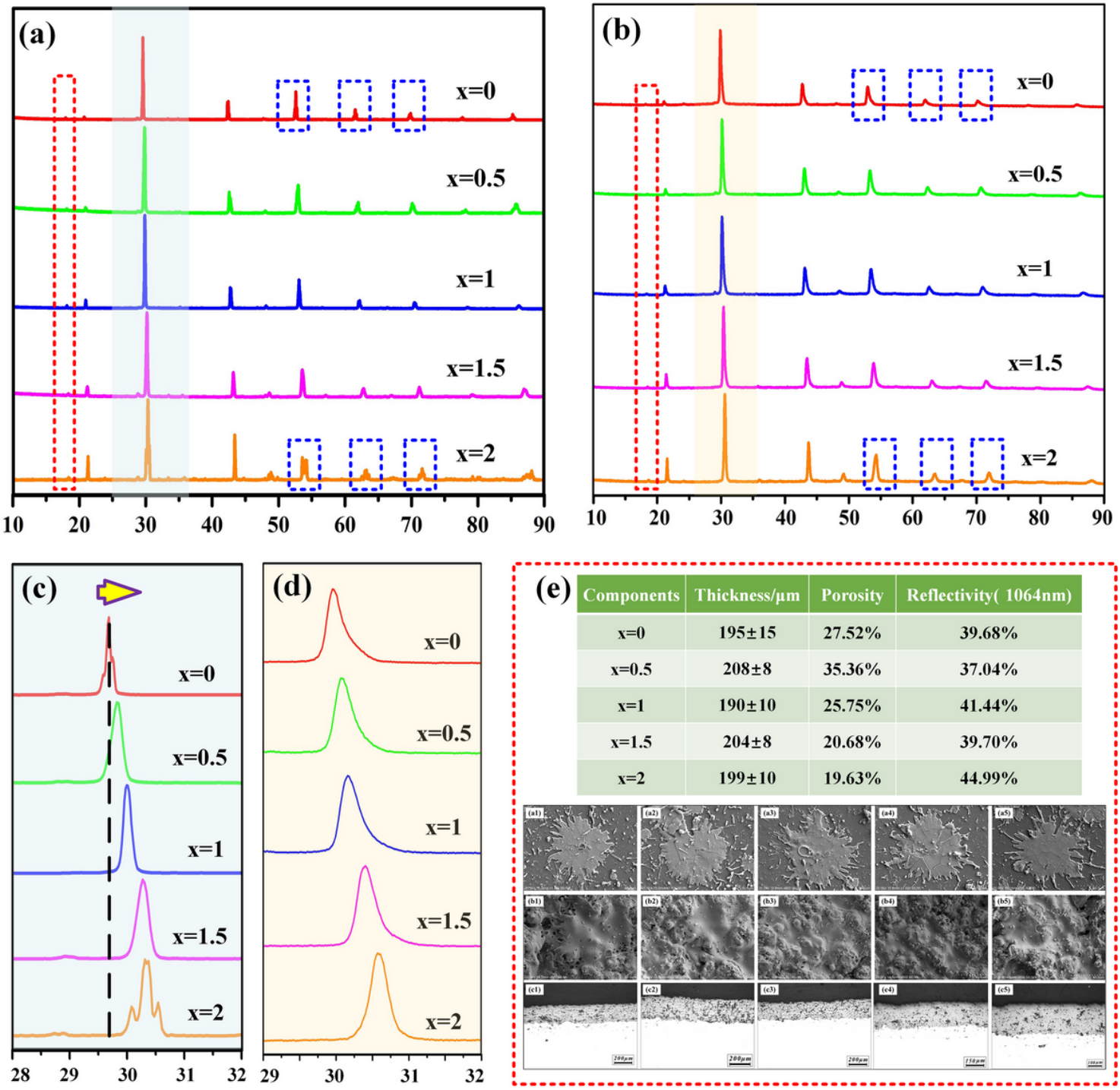

Components	Thickness/μm	Porosity	Reflectivity(1064nm)
x=0	195±15	27.52%	39.68%
x=0.5	208±8	35.36%	37.04%
x=1	190±10	25.75%	41.44%
x=1.5	204±8	20.68%	39.70%
x=2	199±10	19.63%	44.99%

Figure 1

The XRD patterns of Ba2-xSrxSmTaO6 before and after plasma spray and coatings morphology patterns.

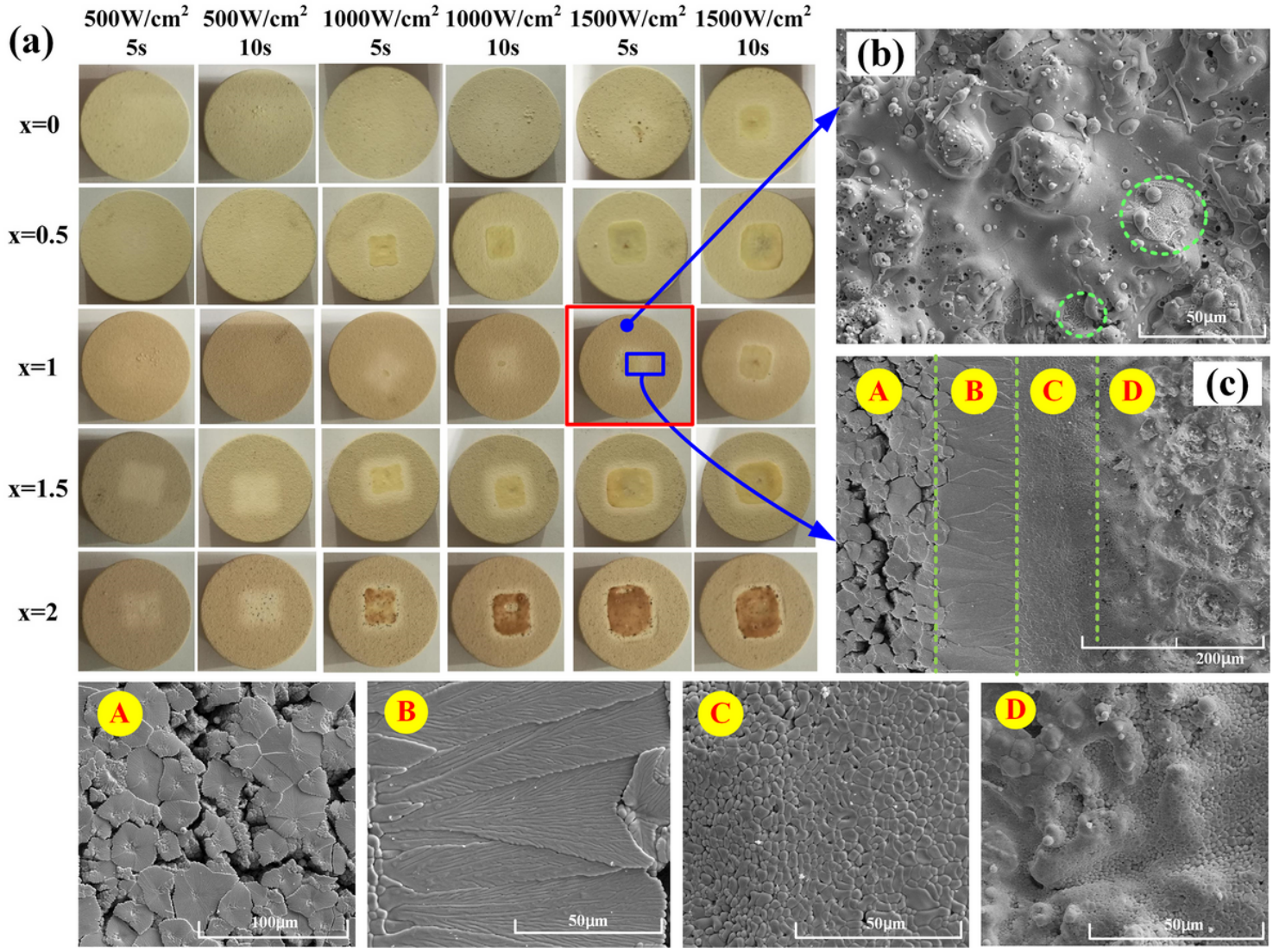

Figure 2

The macro morphology and typical micro morphology of Ba2-xSrxSmTaO6 coatings

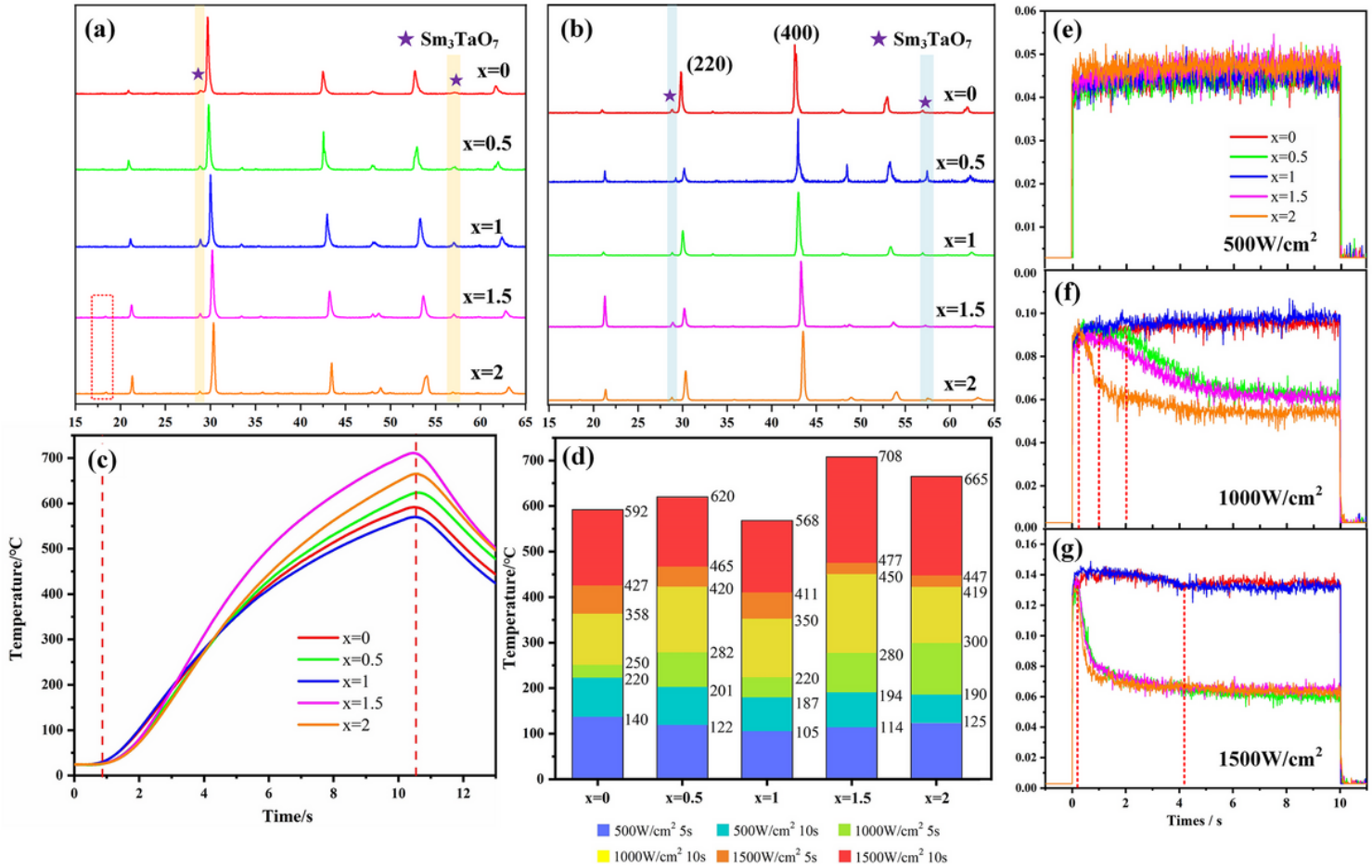

Figure 3

The change of phase structures, back-surface temperatures and front-surface scattered light after and during laser irradiation. (a)The XRD pattern of unmelted region after laser irradiation, (b) the XRD pattern of melted region after laser irradiation, (c) the back-surface temperature during laser irradiation at 1500W/cm2 10s, (d) the maximum back-surface temperature at different irradiation parameters and the front-surface scattered light during laser irradiation at (e)500W/cm2 (f) 1000W/cm2and (g) 1500W/cm2